

---

# Learning Bijective Feature Maps for Linear ICA

---

Alexander Camuto<sup>1 2 \*</sup> Matthew Willetts<sup>1 2 \*</sup> Brooks Paige<sup>1 3</sup> Chris Holmes<sup>1 2</sup> Stephen Roberts<sup>1 2</sup>

## Abstract

Separating high-dimensional data like images into independent latent factors remains an open research problem. Here we develop a method that jointly learns a linear independent component analysis (ICA) model with non-linear bijective feature maps. By combining these two methods, ICA can learn interpretable latent structure for images. For non-square ICA, where we assume the number of sources is less than the dimensionality of data, we achieve better unsupervised latent factor discovery than flow-based models and linear ICA. This performance scales to large image datasets such as CelebA.

## 1. Introduction

In linear Independent Component Analysis (ICA) data is modelled as having been created from linearly mixing together independent latent *sources* (Cardoso, 1989a;b; Jutten & Herault, 1991; Comon, 1994; Bell & Sejnowski, 1995; Cardoso, 1997; Lee et al., 2000). The canonical problem is blind source separation; the aim is to estimate the original sources of a mixed set of signals by learning an *unmixing* or *decorrelating* matrix (we use these terms interchangeably), which when multiplied with data recovers the values of these sources. While linear ICA is a powerful approach to undo the mixing of signals like sound, (Everson & Roberts, 2001; Hyvärinen et al., 2001), it has not been as effectively developed for learning compact representations of high-dimensional data like images, where the linear assumption is limiting. Non-linear ICA methods, where we assume the data has been created from a non-linear mixture of latent sources, offer better performance on such data.

In particular, flow-based models have been proposed as a non-linear approach to square ICA, where we assume the dimensionality of our latent source space is the same as that of our data (Deco & Brauer, 1995; Parra et al., 1995;

1996; Parra, 1996; Dinh et al., 2015; 2017). These flows parameterise a bijective mapping between data and a feature space of the same dimension and can be trained under a maximum likelihood objective for a chosen prior in that space. While such models can create extremely powerful generative models, for most image data one could want to have fewer latent variables than the number of pixels in an image. In such situations, we wish to learn a non-square (dimensionality-reducing) ICA representation over images.

Here we propose a novel methodology for performing non-square ICA using a model with two jointly trained parts: a non-square linear ICA model operating on a feature space output by a bijective flow. The bijective flow is tasked with learning a representation for which linear ICA is a good model. It is as if we are *learning the data* for our ICA model. Further, to induce optimal source separation in our model, we introduce novel theory for the parameterisation of decorrelating, non-square ICA matrices close to the Stiefel Manifold (Stiefel, 1935), the space of orthonormal rectangular matrices. By doing so we introduce a novel non-square linear ICA model which can successfully induce dimensionality reduction in flow-based models and scales non-square non-linear ICA methods to high-dimensional image data.

We show that our hybrid model *Bijecta*, a flow jointly trained with our ICA model, outperforms each of its constituent components in isolation in terms of latent factor discovery. We demonstrate this on the MNIST, Fashion-MNIST, CIFAR-10, and CelebA datasets.

More broadly we demonstrate that:

- By combining bijective mappings with non-square linear ICA we are able to learn a low dimensional ICA source representation for high-dimensional data.
- We show that our method induces concentration of information into a low-dimensional manifold in the bijective space of the flow, unlike flows trained under a standard base distribution.

## 2. Independent Component Analysis

ICA is a highly diverse modelling paradigm with numerous variants: learning a mapping vs learning a model, linear vs non-linear, different loss functions, different generative models, and a wide array of methods of inference

---

\*Equal contribution <sup>1</sup>The Alan Turing Institute, London <sup>2</sup>University of Oxford <sup>3</sup>University College London. Correspondence to: Alexander Camuto <acamuto@turing.ac.uk>, Matthew Willetts <mwillets@turing.ac.uk>.

(Cardoso, 1989a; Jutten & Herault, 1991; Mackay, 1996; Roweis & Ghahramani, 1999; Hyvärinen & Pajunen, 1999; Lee et al., 2000; Lappalainen & Honkela, 2000; Karhunen, 2001). Generally, the goal of ICA is to learn a set of statistically independent sources that ‘explain’ our data.

In this paper, we follow the approach of specifying a generative model and finding point-wise maximum likelihood estimates of model parameters. This variety of ICA starts from demonstrations that earlier infomax-principle (Linsker, 1989) approaches to ICA (Bell & Sejnowski, 1995) are equivalent to maximum likelihood training (Mackay, 1996; Cardoso, 1997; Pearlmutter & Parra, 1997; Roberts, 1998; Everson & Roberts, 1999). Mean-field variational inference for ICA, both for non-linear and linear, has been developed in Lawrence & Bishop (2000); Choudrey (2000); Valpola et al. (2003); Roberts & Choudrey (2004); Honkela & Valpola (2005); Winther & Petersen (2007).

Concretely, we have a model with latent sources  $\mathbf{s} \in \mathcal{S} = \mathbb{R}^{d_s}$  generating data  $\mathbf{x} \in \mathcal{X} = \mathbb{R}^D$ , with  $d_s \leq D$ . The generative model for linear ICA factorises as

$$p_\theta(\mathbf{x}, \mathbf{s}) = p_\theta(\mathbf{x}|\mathbf{s})p(\mathbf{s}), \quad (1)$$

where  $p(\mathbf{s})$  is a set of independent distributions appropriate for ICA,

$$p_\theta(\mathbf{s}) = \prod_{i=1}^{d_s} p_\theta(s_i). \quad (2)$$

In linear ICA, where all mappings are simple matrix multiplications, to enforce identifiability, the priors over the sources *cannot* be Gaussian distributions. Recall that we are mixing our sources to generate our data: A linear mixing of Gaussian random variables is itself Gaussian, so unmixing is impossible (Lawrence & Bishop, 2000). To be able to unmix, to break this symmetry, we can choose any heavy-tailed or light-tailed non-Gaussian distribution as our prior  $p(\mathbf{s})$ . That gives us axis alignment and independence between sources.

### 2.1. Non-Linear ICA

One approach to extend ICA is to have a non-linear mapping acting on the independent sources and data (Burel, 1992; Deco & Brauer, 1995; Yang et al., 1998; Karhunen, 2001; Almeida, 2003; Valpola et al., 2003). In general non-linear ICA models have been shown to be hard to train, having problems of unidentifiability (Hyvärinen & Pajunen, 1999; Karhunen, 2001; Almeida, 2003; Hyvärinen et al., 2019). This means that for a given dataset the model has numerous local minima it can reach under its training objective, with potentially very different learnt sources associated with each.

Some non-linear ICA models have been specified with additional structure, such as putting priors on variables (Lap-

palainen & Honkela, 2000) or specifying the precise non-linear functions involved (Lee & Koehler, 1997; Taleb, 2002), reducing its space of potential solutions. Recent work (Khemakhem et al., 2020) has given a proof that conditioning the source distributions on some always-observed side information, such as time index or class of data, can be sufficient to induce identifiability in non-linear ICA.

### 3. Flows

Flows are models that stack numerous invertible changes of variables. One can then specify a relatively simple base distribution and learn a sequence of (invertible) transforms, defined to have tractable Jacobian matrices, such that one’s data is likely after that mapping.

Given a variable latent variable  $\mathbf{z} \in \mathcal{Z} = \mathbb{R}^D$ , we can specify our distribution over data  $\mathbf{x}$  as

$$p(\mathbf{x}) = p(\mathbf{z}) \left| \det \frac{\partial f^{-1}}{\partial \mathbf{z}} \right|, \quad (3)$$

where  $f$  is a bijection  $\mathbb{R}^D \rightarrow \mathbb{R}^D$  and  $p(\mathbf{z})$  is the base distribution over the latent  $\mathbf{z}$  (Rezende & Mohamed, 2015; Papamakarios et al., 2019). To create more powerful and flexible distributions for  $\mathbf{x}$  we can use the properties of function composition to specify  $\mathbf{x}$  as the a series of transformations of our simple prior  $p$  into a more complex multi-modal distribution, e.g. for a series of  $K + 1$  mappings,

$$\mathbf{z} = f_K \circ \dots \circ f_0(\mathbf{x}). \quad (4)$$

By the properties of determinants under function composition we obtain

$$p(\mathbf{x}) = p(\mathbf{z}_K) \prod_{i=0}^K \left| \det \frac{\partial f_i^{-1}}{\partial \mathbf{z}_{i+1}} \right|, \quad (5)$$

where  $\mathbf{z}_i$  denotes the variable resulting from the transformation  $f_i(\mathbf{z}_i)$ ,  $p(\mathbf{z}_K)$  defines a density on the  $K^{\text{th}}$ , and the bottom most variable is our data ( $\mathbf{z}_0 = \mathbf{x}$ ).

#### 3.1. Coupling Layers

Computing the determinant of the Jacobian,  $\left| \det \frac{\partial f^{-1}}{\partial \mathbf{z}} \right|$ , in Eq. (3) can be prohibitively costly, especially when composing multiple functions as in Eq. (5). To address this, most flows use *coupling layers* that enforce a lower triangular Jacobian such that the determinant of the Jacobian is simply the product of its diagonal elements. We use the coupling layers of Durkan et al. (2019) to enforce this lower triangular structure. For an outline of these coupling layers, see Appendix E.

#### 3.2. Spline Flows

Generally,  $f$  must be bijective to be invertible. A powerful and flexible class of functions that satisfy this requirement

are monotonic rational quadratic splines (RQS) (Durkan et al., 2019).

We use these splines as part of the coupling layers detailed above and parameterise the parameters of these functions using deep neural networks. These networks encode  $K$  monotonically increasing *knots*, which are the coordinate pairs through which the function passes:  $\{(x_k, y_k)\}_{k=0}^K$ . These networks also encode the derivative at each of these knots. Using these parameters we can interpolate values between each of the  $K$  knots using the equation for the RQS transformation detailed in Durkan et al. (2019). The resulting function is highly flexible so RQS flows require fewer composed mappings to achieve good performance relative to other coupling layers.

#### 4. Bijeta: Combining Flows with ICA

We combine linear ICA with a dimensionality-preserving invertible flow  $f_\theta$ . The flow acts between our data space and the representation from the linear ICA generative model.

We want the latent representation to be structured such that it is well fit by the simple, linear ICA model. In some sense, this can be thought of as ‘learning the data’ for an ICA model, where the ‘data’ the ICA model acts on is the output of the invertible feature map defined by the flow. The inferred latent sources of the ICA model can have a lower dimensionality than the data or flow representation.

We choose our base ICA source distribution, and the ICA generative likelihood, to be multivariate Laplace distributions (Everson & Roberts, 2001). To be clear, the result of this mixing of sources is not our data, but an intermediate representation  $\mathbf{z}$  which interacts with a flow that maps it to data.

$$p_\theta(s_i) = \text{Laplace}(s_i|0, 1), \text{ for } i = 1, \dots, d_s \quad (6)$$

$$p_\theta(\mathbf{z}|\mathbf{s}) = \text{Laplace}(\mathbf{z}|\mathbf{A}\mathbf{s}, \mathbf{b}), \quad (7)$$

where  $\mathbf{A} \in \mathbb{R}^{D \times d_s}$  is our (unknown) ICA mixing matrix, which acts on the sources to produce a linear mixture; and  $\mathbf{b}$  is a learnt or fixed diagonal diversity.

Our model has the three sets of variables: the observed data  $\mathbf{x}$ , the flow representation  $\mathbf{z} = f(\mathbf{x})$ , and ICA latent sources  $\mathbf{s}$ . It can be factorised as

$$p_\theta(\mathbf{x}, \mathbf{s}) = p_\theta(\mathbf{x}|\mathbf{s})p_\theta(\mathbf{s}) \quad (8)$$

$$= p_\theta(\mathbf{z}|\mathbf{s})p_\theta(\mathbf{s}) \left| \det \frac{\partial f^{-1}}{\partial \mathbf{z}} \right|. \quad (9)$$

To train the ICA part of the model by maximum likelihood we would marginalise out  $\mathbf{s}$  and evaluate the evidence in  $\mathcal{Z}$ :

$$p(\mathbf{z}; \mathbf{A}, \Sigma) = \int d\mathbf{s} p(\mathbf{z}|\mathbf{s}; \mathbf{A})p(\mathbf{s}) \quad (10)$$

This marginal is intractable. We propose a contemporary approach for approximate inference in linear ICA, using advances in amortised variational inference. This means we introduce an approximate amortised posterior for  $\mathbf{s}$  and perform importance sampling on Eq (10), taking gradients through our samples using the reparameterisation trick (Kingma & Welling, 2014; Rezende et al., 2014).

By training this model using amortised stochastic variational inference we gain numerous benefits. Training scales to large datasets using stochastic gradient descent, and we are free to choose the functional and probabilistic form of our approximate posterior. We choose a linear mapping in our posterior, with

$$q_\phi(\mathbf{s}|\mathbf{z}) = \text{Laplace}(\mathbf{s}|\mathbf{A}^+\mathbf{z}, \mathbf{b}_\phi), \quad (11)$$

where we have introduced variational parameters  $\phi = \{\mathbf{A}^+, \mathbf{b}_\phi\}$  corresponding to an unmixing matrix and a diagonal diversity.

We use samples from this posterior to define a lower bound  $\mathcal{L}$  on the evidence in  $\mathcal{Z}$

$$\begin{aligned} \log p(\mathbf{z}; \mathbf{A}, \Sigma) &\geq \mathcal{L}(\mathbf{z}; \phi, \mathbf{A}, \Sigma) \quad (12) \\ &= \mathbb{E}_{\mathbf{s} \sim q} [\log p(\mathbf{z}|\mathbf{s}; \mathbf{A}) - \text{KL}(q_\phi(\mathbf{s}|\mathbf{z}; \mathbf{A})||p(\mathbf{s}))] \end{aligned}$$

Using the change of variables equation, Eq (3), and this lower bound on the evidence in  $\mathcal{Z}$ , we can obtain a variational lower bound on the evidence for our data  $\mathbf{x}$  as the sum of the ICA model’s ELBO (acting on  $\mathbf{z}$ ) and the log determinant of the flow:

$$\log p_\theta(\mathbf{x}; \mathbf{A}, \mathbf{b}) \geq \mathcal{L}(\mathbf{x}; \theta, \phi, \mathbf{A}, \mathbf{b}) \quad (13)$$

$$= \mathcal{L}(\mathbf{z}; \phi, \mathbf{A}, \mathbf{b}) + \log \left| \det \frac{\partial f_\theta^{-1}}{\partial \mathbf{z}} \right|. \quad (14)$$

As such our model is akin to a flow model, but with an additional latent variable  $\mathbf{s}$ ; the base distribution  $p(\mathbf{z})$  of the flow is defined through marginalizing out the linear mixing of the sources. We refer to a model with  $n$  non-linear splines mapping from  $\mathcal{X}$  to  $\mathcal{Z}$  as an  $n$ -layer Bijeta model.

In the case of non-square ICA, where our ICA model is not perfectly invertible, errors when reconstructing a mapping from  $\mathcal{S}$  to  $\mathcal{Z}$  may amplify when mapping back to  $\mathcal{X}$ . We additionally penalise the  $L_1$  error of each point when reconstructed into  $\mathcal{X}$  as an additional regularisation term in our loss. This penalisation can be weighted according to the importance of high-fidelity reconstructions for a given application.

#### 5. Manifolds for the unmixing matrix $\mathbf{A}^+$

What are good choices for the mixing and unmixing matrices? As we will show, design choices as to the parameterisation of  $\mathbf{A}^+$  can accelerate the convergence of our flow-based

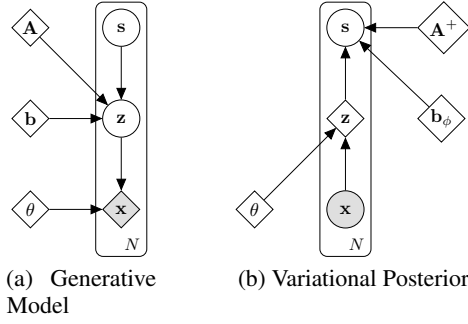


Figure 1. The generative model (a) and variational posterior (b), as defined in Eq (14).

ICA model, and provide guarantees on the structure of the learnt projections.

Before discussing how to pick unmixing matrices for non-square linear ICA, first we briefly cover the square case, where the number of generative factors is equal to the dimensionality of our data space,  $d_s = D$ . This assumption greatly simplifies the construction of the unmixing matrix. Generally, members of the orthogonal group  $O(n)$  group have been shown to be optimal for decorrelating ICA sources; with sufficient data the maximum likelihood unmixing matrices lies on this decorrelating manifold and will be reached by models confined to this manifold (Everson & Roberts, 1999).

Thus we constrain  $\mathbf{A}^+$  to belong to the Lie group of special orthogonal matrices  $SO(D)$  with determinant 1. We want to perform unconstrained optimisation in learning our matrix, so we wish to use a differentiable transformation from a class of simpler matrices to the class of orthogonal matrices.

For a given anti-symmetric matrix  $\mathbf{M}$  (i.e., satisfying  $\mathbf{M} = -\mathbf{M}^T$ ), its Cayley Transform (Cayley, 1846) is a member of  $SO(D)$ . As such, we propose defining our square unmixing matrix as the Cayley transform of the anti-symmetric matrix  $\mathbf{M}$ ,

$$\mathbf{A}^+ = (\mathbf{I} - \mathbf{M})^{-1}(\mathbf{I} + \mathbf{M}). \quad (15)$$

This can be formulated as an unconstrained problem, easing optimization, by defining  $\mathbf{M} = (\mathbf{L} - \mathbf{L}^T)/2$  and then optimizing over the square real-valued matrix  $\mathbf{L}$ .

### 5.1. $\mathbf{A}^+$ for non-square ICA

Intuitively, for non-square ICA our aim is to construct an unmixing matrix that is approximately orthogonal, such that  $\mathbf{A}^+$  has the decorrelating properties we observe when constraining it to lie on  $SO(D)$  in the case of square ICA. Here we propose a new method for non-square ICA, combining ideas from sketching (Woodruff, 2014) with these manifold-learning approaches.

The set of rectangular matrices  $\mathbf{G}$  that are exactly orthogonal, i.e. that fulfill  $\mathbf{G}\mathbf{G}^* = \mathbf{I}$  ( $\mathbf{G}^*$  the conjugate transpose of  $\mathbf{G}$ ) lie on the Stiefel Manifold (Stiefel, 1935; Edelman et al., 1998). For a given number of rows and columns  $r, c$ , such a manifold is denoted  $\mathcal{V}(r, c)$ . We wish to specify our rectangular unmixing matrix  $\mathbf{A}^+$  of dimensionality  $d_s \times D$  to be approximately-Stiefel, lying close to  $\mathcal{V}(d_s, D)$ . This choice is justified by the following theorem which we prove in Appendix B:

**Theorem 1** *As the Frobenius norm  $\|\mathbf{G} - \tilde{\mathbf{G}}\| \rightarrow 0$ , where  $\mathbf{G} \in \mathbb{R}^{r \times c}$  and  $\tilde{\mathbf{G}}$  is the projection of  $\mathbf{G}$  onto  $\mathcal{V}(r, c)$ ,  $\|\mathbf{G}\mathbf{X}\mathbf{X}^T\mathbf{G}^T - \mathbf{D}\| \rightarrow 0$ , where  $\mathbf{G}\mathbf{X}\mathbf{X}^T\mathbf{G}^T$  is the cross-correlation of the projection of data  $\mathbf{X}$  by  $\mathbf{G}$ , and  $\mathbf{D}$  is some diagonal matrix.*

More simply this shows that as a matrix  $\mathbf{G} \in \mathbb{R}^{r \times c}$  approaches  $\mathcal{V}(r, c)$  the off diagonal elements of the cross-correlation matrix,  $\mathbf{G}\mathbf{X}\mathbf{X}^T\mathbf{G}^T$ , become smaller in magnitude and we achieve independent projections  $\mathbf{S} = \mathbf{G}\mathbf{X}$ .

In the case of non-square ICA, the dimensionality of our latent space is less than the dimensionality of our data space, so  $\mathbf{A}^+$  cannot in general form a bijection. We need  $\mathbf{A}^+$  to compress from  $\mathbb{R}^D$  to  $\mathbb{R}^{d_s}$  and we need it to perform a rotation such that the learnt latent sources align with the axis-aligned priors we impose in  $\mathcal{S}$ . We decompose

$$\mathbf{A}^+ = \mathbf{R}\mathbf{Q}, \quad (16)$$

each part doing one of these tasks. The projection matrix  $\mathbf{Q} \in \mathbb{R}^{d_s \times D}$  handles the dimensionality reduction, while  $\mathbf{R} \in \mathbb{R}^{d_s \times d_s}$  performs unmixing in  $\mathcal{S}$ . In essence,  $\mathbf{R}$  is our decorrelating matrix and  $\mathbf{Q}$  is our projection matrix. We make specific choices for the structure of both these matrices, which can ensure the resulting  $\mathbf{A}^+$  lies close to the manifold  $\mathcal{V}(d_s, D)$ , while still permitting us to perform optimisation in an unconstrained parameter space.

**The  $SO(D)$  Lie group for  $\mathbf{R}$ :** Because  $\mathbf{R}$  is a square matrix we can constrain it to belong to  $SO(\cdot)$  as in the case of square ICA. By doing so we ensure  $\mathbf{R}$  has the decorrelating properties we are seeking.

$$\mathbf{R} = (\mathbf{I} - \mathbf{M})^{-1}(\mathbf{I} + \mathbf{M}) \quad (17)$$

Where  $\mathbf{M}$  is an anti-symmetric matrix as detailed in Section 5.

**$\mathbf{Q}$  for an approximately Stiefel  $\mathbf{A}^+$ :** Our goal is to construct a rectangular matrix  $\mathbf{A}^+$  such that  $\mathbf{A}^+(\mathbf{A}^+)^T \approx \mathbf{I}$  and  $(\mathbf{A}^+)^T\mathbf{A}^+ \approx \mathbf{I}$ . As stated above, we constrain  $\mathbf{R}$ , one part of  $\mathbf{A}^+$  to be *exactly* orthogonal. For our compressive matrix,  $\mathbf{Q}$ , our goal is to constrain it to be *approximately* orthogonal. The justification for this is provided by the following theorem:

**Theorem 2** For  $\mathbf{A}^+ = \mathbf{R}\mathbf{Q}$ ,  $\mathbf{R} \in SO(d_s)$ ,  $\mathbf{Q} \in \mathbb{R}^{d_s \times D}$ , as the Frobenius norm  $\|\mathbf{Q}\mathbf{Q}^T - \mathbf{I}\| \rightarrow 0$ , we also have  $\|\tilde{\mathbf{A}}^+ - \mathbf{A}^+\| \rightarrow 0$ , where  $\tilde{\mathbf{A}}^+$  is the projection of  $\mathbf{A}^+$  onto  $\mathcal{V}(d_s, D)$ .

The proof of this theorem is in Appendix A. If  $\mathbf{Q}$  satisfies  $\mathbf{Q}\mathbf{Q}^T \approx \mathbf{I}$ , then  $\mathbf{A}^+$  lies close to  $\mathcal{V}(d_s, D)$  by Theorem 2, and by Theorem 1 we can deduce  $\mathbf{A}^+$  will have decorrelating properties.

Recall that our optimisation space for  $\mathbf{A}^+$  lies in  $\mathbb{R}^{d_s \times D}$ . For large dimensional data such as images this can constitute a prohibitively large search space for an approximately orthogonal matrix. We can choose to fix  $\mathbf{Q}$  such that optimisation occurs in  $\mathbb{R}^{d_s \times d_s}$  space, solely for the matrix  $\mathbf{R}$ . For most non-square ICA problems we assume that  $d_s \ll D$  and fixing  $\mathbf{Q}$  can greatly accelerate optimisation without limiting the space of solutions for the unmixing matrix  $\mathbf{R}$ .

Such approximately orthogonal matrices can be constructed very cheaply by way of Johnson-Lindenstrauss (JL) Projections (Johnson & Lindenstrauss, 1984; Dasgupta & Gupta, 2003). We draw  $\mathbf{Q}$  once from one such projection at initialisation and leave it fixed for the remainder of training.

### Johnson-Lindenstrauss Projections

One can obtain a JL projection for  $\mathbb{R}^D \rightarrow \mathbb{R}^{d_s}$  by sampling from a simple binary distribution (Achlioptas, 2003):

$$Q_{i,j} = \begin{cases} +\frac{1}{\sqrt{d_s}}, & \text{with probability } \frac{1}{2} \\ -\frac{1}{\sqrt{d_s}}, & \text{with probability } \frac{1}{2} \end{cases} \quad (18)$$

This distribution satisfies  $\mathbb{E}[\mathbf{Q}\mathbf{Q}^T] = \mathbf{I}$ , and as Achlioptas (2003) show, such a draw has  $\mathbf{Q}\mathbf{Q}^T \approx \mathbf{I}$ ; then by Theorems 1 and 2 we know  $\mathbf{A}^+$  will be a decorrelating matrix.

### 5.2. The mixing matrix $\mathbf{A}$

The mixing matrix  $\mathbf{A}$  requires fewer constraints than  $\mathbf{A}^+$ , the unmixing matrix. For non-square ICA we construct  $\mathbf{A}$  as the product

$$\mathbf{A} = \mathbf{B}\mathbf{R}^T, \quad (19)$$

where  $\mathbf{R}^T \in \mathbb{R}^{d_s \times d_s}$  is exactly the transpose of the unmixing component of  $\mathbf{A}^+$ , and the matrix  $\mathbf{B} \in \mathbb{R}^{D \times d_s}$  is unconstrained. We are essentially using the inverse of the unmixing matrix and projecting it from  $\mathcal{S}$  space to  $\mathcal{Z}$  space by way of  $\mathbf{B}$ .

## 6. Experiments

A good unsupervised ICA model is one that can: learn useful and informative latent representations; produce realistic-looking samples; and well approximate the underlying data distribution. Here we show that Bijecta outperforms both

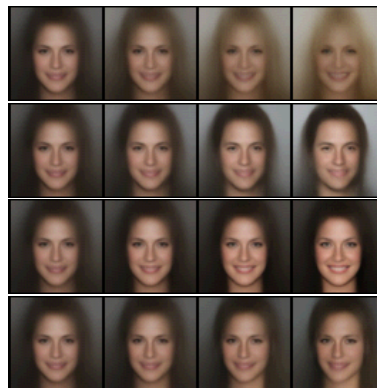


Figure 2. Four axis-aligned latent-space traversals for a 12 layer Bijecta with  $d_s = 512$  trained on CelebA. Images to the left correspond to the original sample from the base distribution. As we move to the right these images correspond to linearly increasing values along a single latent dimension up to 10 standard deviations away whilst the other dimensions remain fixed. The first dimension encodes hair-color, the second gender, the third the degree of smiling and the fourth rotation. Most striking is the fact that these transforms are identity preserving: as we vary along one axis it is apparent that the features that are core to the original face are retained. In standard flow-based models, such transforms are typically not axis-aligned and most transformations in flow latent spaces are not identity preserving.

flows with fixed base distributions and linear ICA models by these criteria.

### 6.1. Likelihood Collapse

Our model is rewarded for learning representations  $\mathbf{z}$  that can be readily decorrelated by a linear ICA model. This presents some unique modes of failure which we observed when training these models. Under the objective we defined in Eq (14), a trivial solution for a flow model is to have a highly peaked distribution over reconstructions. For a given flow embedding  $\mathbf{z}^*$ ,  $r(\mathbf{z}|\mathbf{z}^*) = \int ds p(\mathbf{z}|\mathbf{s}; \mathbf{A})q(\mathbf{s}|\mathbf{z}^*)$ , collapses to a distribution with zero mean and a variance that is greater than the variance of the likelihood distribution, and in fact hardly depends on the input  $\mathbf{z}^*$ . Under this collapse, where  $r(\mathbf{z}|\mathbf{z}^*)$  is of low variance, the ICA model estimates  $p(\mathbf{z}|\mathbf{s})$  to be a distribution with mean close to 0 and with greater variance than the appropriate embedding-dependent  $p(\mathbf{z}|\mathbf{s})$ , for *all* datapoints. Because the values of  $\mathbf{z}$  have collapsed to 0 under the flow model, we obtain high likelihood values even if reconstructions and samples are poor.

To prevent this *likelihood collapse*, we add a final  $L_1$  normalising layer to our flow  $f$ , which prevents the variance of  $\mathbf{z}$  from drifting. Such layers ensure that data batches have zero mean and unit variance and prevent variance collapse. Each component  $x_k$ ,  $k = 1 \dots D$  of the input to this layer  $\mathbf{x}$

is rescaled in the following fashion:

$$x_k = \frac{x_k - \mu_k}{\sqrt{\frac{\pi}{2}} \|x_k - \mu_k\|_1 / n} \quad (20)$$

where  $n$  is the batch size,  $\mu_k$  is the batch mean over component  $k$ . As Hoffer et al. (2018) show, the expected value of the denominator is the data standard deviation  $\sigma$ . As such we are enforcing unit variance. The log determinant of the Jacobian of this layer is simply the negative log of the denominator in Eq (20),  $-\log(\sqrt{\frac{\pi}{2}} \|x_k - \mu_k\|_1 / n)$ .

To calculate batch statistics when generating data from our model, when we do not have an input  $\mathbf{x}$ , we keep a running average that is reminiscent of batch norm layers in neural networks (Ioffe & Szegedy, 2015). The running mean and standard deviation for the layer at step  $t + 1$  of training are:

$$\begin{aligned} \boldsymbol{\mu}_{t+1} &= (1 - \rho)\boldsymbol{\mu}_t + \rho\boldsymbol{\mu}_b \\ \boldsymbol{\sigma}_{t+1} &= (1 - \rho)\boldsymbol{\sigma}_t + \rho\boldsymbol{\sigma}_b \end{aligned}$$

where  $\boldsymbol{\mu}_b$  and  $\boldsymbol{\sigma}_b$  are the statistics calculated over the current training batch and  $\rho$  is a momentum term which regulates the variance at each update. These statistics are then used to calculate the inverse of the layer when generating data.

## 6.2. Results and Discussion

### 6.2.1. DIMENSIONALITY REDUCTION ON FLOW MODELS

We first contrast our model’s ability to automatically uncover sources relative to flow models with heavy-tailed base distributions. We do so by measuring the cumulative explained variance by the dimensions in  $\mathcal{Z}$  for both these models. If a small number of dimensions explains most of  $\mathcal{Z}$ ’s variance then the model has learnt a bijection which only requires a small number of dimensions to be invertible. It has in effect learnt the generating sources underpinning the data.

In Figure 3 we demonstrate that Bijecta is able to induce better-compressed representations in  $\mathcal{Z}$  than a non-compressive flow on CIFAR-10 and Fashion-MNIST datasets. We compute the eigenvalues of the covariance matrix on the output of the flow, i.e. on  $\text{Cov}(f(\mathbf{X}))$ , to see how much of the total variance in the learned feature space  $\mathcal{Z}$  can be explained in a few dimensions. In doing so we see that our flows trained jointly with a linear ICA model with  $d_s = 64$  effectively concentrates variation into a small number of intrinsic dimensions; this is in stark contrast with the RQS flows trained with only a simple Laplace base distribution. This demonstrates that our model is capable of automatically detecting relevant directions on a low dimensional manifold in  $\mathcal{Z}$ , and that the bijective component of our model is better able to isolate latent sources than a standard flow.

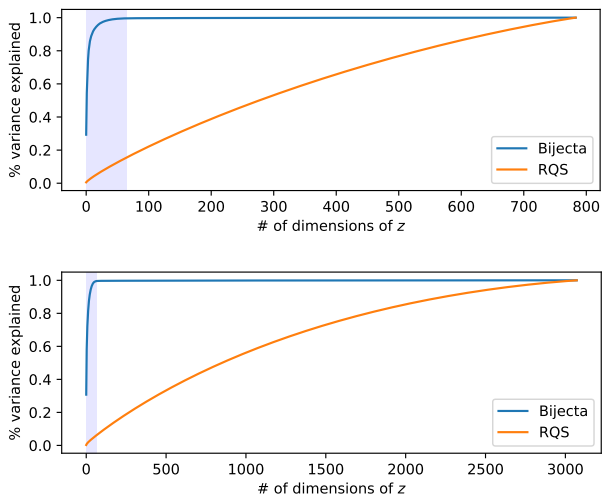


Figure 3. Explained variance plots for the embedding in  $\mathcal{Z}$ , as measured by the sums of the eigenvalues of the covariance matrix of the embeddings, for both our Bijecta model and for an RQS model trained with a Laplace base distribution. For both Fashion-MNIST (top) and CIFAR 10 (bottom) datasets we see that the Bijecta model has learned a compressive flow, where most of the variance can be explained by only a few linear projections. The shaded region denotes the first 64 dimensions, corresponding to the size of the target source embedding  $\mathcal{S}$ .

### 6.2.2. VISUALISATION OF LEARNT LATENT FACTORS

For a visual illustration of this source separation we show the difference in generated images resulting from smoothly varying along each dimension in  $\mathcal{S}$  for Bijecta models and in  $\mathcal{Z}$  for flow models. Bijecta’s ability to discover latent sources is highlighted visually in Figures 2 and 4, where our model is clearly able to learn axis-aligned transformations of CelebA faces, whereas a flow trained with equivalent computational budget does not. This improvement in source discovery translates into our model’s ability to more quickly converge to a well-conditioned generative model under a heavy-tailed prior, which is highlighted by the samples drawn from Bijecta and RQS flows in Figure 4.

### 6.2.3. IMPROVING LINEAR ICA USING BIJECTIVE MAPS

Having ascertained the benefit of using our model for source discovery relative to a flow with a heavy-tailed prior, we demonstrate the benefit of using a bijective map to improve on the performance of linear ICA. We do so by measuring metrics which assess the independence of a model’s uncovered factors in  $\mathcal{S}$  and the quality of a model’s compressed representation, generally evaluated by determining a model’s ability to reconstruct an input from a compressed embedding in  $\mathcal{S}$ . Table 1 shows the dramatic improvement in such metrics when adding a *single* bijective mapping to linear ICA. This table also shows that improvements scale



Figure 4. Plots comparing samples drawn from Bijecta and RQS flows. Samples from a 1-layer Bijecta (b) with  $d_s = 64$  are contrasted with samples from 1 (c) and 4-layer (d) RQS flows trained with a Laplace base distribution after 25000 training steps. It is apparent that our model has more quickly converged to a well-conditioned generative model, even when compared against a larger baseline. We also show latent traversals moving along 5 latent directions in a 4-layer RQS flow for an embedded training-set point (a). Images in the center correspond to the original sample from the latent space prior. As we move to the right or left these images correspond to linearly increasing values along a single latent dimension up to 10 standard deviations away whilst the other dimensions remain fixed. Note that though we have selected 5 dimensions, all dimensions in  $\mathcal{Z}$  had similar latent traversals. It is apparent the flow has not discovered axis aligned transforms.

as we stack non-linear mappings.

Such improvements can be appraised visually in figure F.6, which highlights the better reconstructions and sample generation when introducing a single bijective layer. For other examples of such reconstructions see Appendix F. As before, we show latent traversal plots for flows and linear ICA models in Appendix F for CelebA. It is apparent that our models are better able to learn axis-aligned transforms in  $\mathcal{S}$ .

Viewed as a whole, these results show that the bijective map induces a representation that is better decorrelated by a linear mapping and is also easier to reconstruct under this linear mapping.

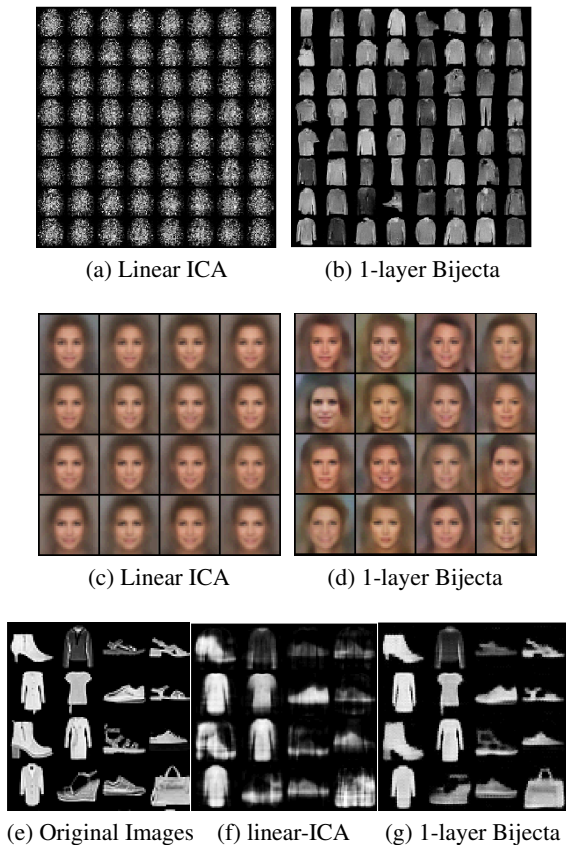


Figure 5. Plots comparing samples and reconstructions from Bijecta and linear ICA models with  $d_s = 64$ . Here we show samples drawn from the generative model of linear-ICA and a 1-layer Bijecta model trained on fashion-MNIST (a), (b) and CelebA (c), (d). The superior quality and most importantly the greater diversity of the samples drawn from our model is very apparent. Subfigures (e), (f), (g) show reconstructions from a linear-ICA model and a 1-layer Bijecta model trained on fashion-MNIST. The introduction of the bijective non-linearity significantly improves the quality of reconstructions of linear-ICA.

### 6.3. Methods

All non-square linear-ICA baselines are trained under the objective detailed in Eq. (12) but with no flow so  $\mathbf{z} = \mathbf{x}$ . We construct the mixing and unmixing matrices as detailed in section 5 and they differ from our Bijecta model solely in their lack of bijective mapping that preprocesses data. Similarly, all flow-based baselines are trained using the objective in Eq (5). We match these baselines to the bijective maps of our models in terms of size, neural network architectures, and the presence of normalising layers. Note that unless specified otherwise, all compressive models use a latent space size of 64. Training hyperparameters and network architectures are detailed in Appendix G.

		CIFAR-10	MNIST	fashion-MNIST	CELEBA
Linear-ICA	$\log p(\mathbf{s})/d_s$	-4.8	-4.29	-3.0	-9.0
	$L_1$ reconstruction error in $\mathcal{X}$	3.0	3.1	2.9	2.9
	$L_2$ reconstruction error in $\mathcal{X}$	27.0	32.9	17.3	57.2
1-layer Bijecta	$\log p(\mathbf{s})/d_s$	<b>-4.2</b>	<b>-2.8</b>	<b>-2.2</b>	<b>-7.3</b>
	$L_1$ reconstruction error in $\mathcal{X}$	2.0	1.0	1.6	1.9
	$L_2$ reconstruction error in $\mathcal{Z}$	5.6	4.6	3.8	13.0
4-layer Bijecta	$\log p(\mathbf{s})/d_s$	-4.7	-3.0	<b>-2.2</b>	-7.8
	$L_1$ reconstruction error in $\mathcal{X}$	<b>1.9</b>	<b>0.6</b>	<b>1.2</b>	<b>1.4</b>
	$L_2$ reconstruction error in $\mathcal{Z}$	<b>5.1</b>	<b>3.0</b>	<b>2.4</b>	<b>10.1</b>

Table 1. Here we evaluate the source-separation and reconstruction quality of non-square ICA models. The best performing results are highlighted in bold. We evaluate source separation under a given model by evaluating the mean log probability of the validation set embeddings in  $\mathcal{S}$  under our heavy-tailed prior, normalised by the dimensionality of  $\mathcal{S}$  space:  $\log p(\mathbf{s})/d_s$  ( $d_s = 64$ ). As our base distribution is heavy-tailed, this metric evaluates the axis-alignment, i.e the *independence*, of uncovered factors. We also evaluate the quality of compressed representations using the  $L_2$  reconstruction error from the linear component of each model. In Bijecta this corresponds to the reconstruction error in  $\mathbf{z}$ ; in linear ICA, this corresponds to reconstruction error in  $\mathbf{x}$ . Generally, this highlights a model’s ability to reconstruct linearly compressed data. We also evaluate the quality of compressed representations by measuring the  $L_1$  reconstruction error in  $\mathcal{X}$ . Generally, a better compression encodes more information in  $\mathcal{S}$ , making it easier for the model to then reconstruct in  $\mathcal{Z}$  and subsequently in  $\mathcal{X}$ . Most striking is the improvement across all metrics when introducing a *single* bijective mapping. In particular the lower linear model  $L_2$  reconstruction error coupled with high  $\log p(\mathbf{s})/d_s$  are clear indicators of better source separation. The low linear model  $L_2$  error in  $\mathcal{Z}$  for Bijecta models means the flow component of our models has learnt a representation under which the linear-ICA model can more easily separate sources and reconstruct inputs (also seen by the decrease in  $L_1$  reconstruction error in data space  $\mathcal{X}$ ). Our 4-layer model further improves the quality of the compressed representations as seen by the lower reconstruction errors.

## 7. Related Work

Modern flow-based models were originally proposed as an approach to non-linear square ICA (Dinh et al., 2015), but are also motivated by desires in generative modelling for more expressive priors and posteriors (Kingma et al., 2016; Papamakarios et al., 2019). There were similar early approaches, known as symplectic maps (Deco & Brauer, 1995; Parra et al., 1995; 1996; Parra, 1996), which were also proposed for use with ICA. Overall they offer a variety of expressive dimensionality-preserving (and sometimes volume-preserving) bijective mappings (Dinh et al., 2017; Kingma & Dhariwal, 2018; Papamakarios et al., 2019).

Orthogonal transforms have been used in normalizing flows before, to improve the optimization properties of Sylvester flows (Van Den Berg et al., 2018; Golinski et al., 2019). The latter work also uses a Cayley map to parameterise orthogonal matrices. Here our analysis is flow-agnostic and works with state of the art non-volume preserving flows. Researchers have also looked at imposing Stiefel-manifold structure on the weights of neural networks (Li et al., 2020).

Disentangling, potentially synonymous with non-linear non-square ICA, occurs when there is a one-to-one correspondence between dimensions of a latent space and some human-interpretable features in data generated by the model. Intuitively this means that smoothly varying along an axis-aligned direction in a model’s latent space  $\mathcal{Z}$  should result

in smooth changes in a single feature of the data (Higgins et al., 2017). There are Variational Autoencoder (Rezende et al., 2014; Kingma & Welling, 2014) derived models that obtain this, commonly by upweighting components of their training objective that are associated with statistical independence of their latent distributions (Higgins et al., 2017; Burgess et al., 2017; Kim & Mnih, 2018; Chen et al., 2018; Esmaeili et al., 2019). Khemakhem et al. (2020) prove that in non-linear ICA, latent variables that are not conditioned on other variables cannot produce disentangled representations, but that by conditioning the prior on additional supervised information the model can become identifiable.

## 8. Conclusion

Here we have developed a method for performing non-linear ICA which combines state-of-the-art flow-based models and a novel theoretically grounded non-square linear ICA method. Not only is our model able to learn a representation under which sources are separable by linear unmixing; we have also shown that the flow component concentrates information into a low dimensional manifold in its representation space  $\mathcal{Z}$ . We have also demonstrated the value of our method for latent factor discovery on large high-dimensional image datasets. Bijecta learns a low dimensional, explanatory set of latent representations in  $\mathcal{S}$  as demonstrated by our latent traversals, and draws from the model are realistic-looking.



## References

- Absil, P. A. and Malick, J. Projection-like retractions on matrix manifolds. *SIAM Journal on Optimization*, 22(1):135–158, 2012. ISSN 10526234. doi:10.1137/100802529.
- Achlioptas, D. Database-friendly random projections: Johnson-Lindenstrauss with binary coins. In *Journal of Computer and System Sciences*, volume 66, pp. 671–687, 2003. doi:10.1016/S0022-0000(03)00025-4.
- Almeida, L. B. MISEP – Linear and Nonlinear ICA Based on Mutual Information. *Journal of Machine Learning Research*, 4:1297–1318, 2003.
- Bell, A. J. and Sejnowski, T. J. An information-maximisation approach to blind separation and blind deconvolution. *Neural Computation*, 7(6):1004–1034, 1995.
- Burel, G. Blind separation of sources: A nonlinear neural algorithm. *Neural Networks*, 5(6):937–947, 1992. ISSN 08936080. doi:10.1016/S0893-6080(05)80090-5.
- Burgess, C. P., Higgins, I., Pal, A., Matthey, L., Watters, N., Desjardins, G., Lerchner, A., and London, D. Understanding disentangling in  $\beta$ -VAE. In *NeurIPS*, 2017.
- Cardoso, J. F. Blind identification of independent components with higher-order statistics. In *IEEE Workshop on Higher-Order Spectral Analysis*, 1989a.
- Cardoso, J. F. Source separation using higher order moments. In *ICASSP, IEEE International Conference on Acoustics, Speech and Signal Processing - Proceedings*, volume 4, pp. 2109–2112, 1989b. doi:10.1109/icassp.1989.266878.
- Cardoso, J. F. Infomax and Maximum Likelihood for Blind Source Separation. *IEEE Letters on Signal Processing*, 4: 112–114, 1997.
- Cayley, A. Sur quelques propriétés des déterminants gauches. *Journal für die reine und angewandte Mathematik*, 32:119–123, 1846.
- Chen, R. T. Q., Li, X., Grosse, R., and Duvenaud, D. Isolating Sources of Disentanglement in Variational Autoencoders. In *NeurIPS*, 2018.
- Choudrey, R. *Variational Methods for Bayesian Independent Component Analysis*. PhD thesis, University of Oxford, 2000.
- Comon, P. Independent component analysis, A new concept? *Signal Processing*, 36(3):287–314, 1994. ISSN 01651684. doi:10.1016/0165-1684(94)90029-9.
- Dasgupta, S. and Gupta, A. An Elementary Proof of a Theorem of Johnson and Lindenstrauss. *Random Structures and Algorithms*, 22(1):60–65, 2003. ISSN 10429832. doi:10.1002/rsa.10073.
- Deco, G. and Brauer, W. Higher Order Statistical Decorrelation without Information Loss. In *NeurIPS*, 1995.
- Dinh, L., Krueger, D., and Bengio, Y. NICE: Non-linear Independent Components Estimation. In *ICLR*, 2015.
- Dinh, L., Sohl-Dickstein, J., and Bengio, S. Density estimation using Real NVP. In *ICLR*, 2017.
- Durkan, C., Bekasov, A., Murray, I., and Papamakarios, G. Neural Spline Flows. In *NeurIPS*, 2019.
- Edelman, A., Arias, T. A., and Smith, S. T. The geometry of algorithms with orthogonality constraints. *SIAM Journal on Matrix Analysis and Applications*, 20(2):303–353, 1998. ISSN 08954798. doi:10.1137/S0895479895290954.
- Esmaeili, B., Wu, H., Jain, S., Bozkurt, A., Siddharth, N., Paige, B., Brooks, D. H., Dy, J., and van de Meent, J.-W. Structured Disentangled Representations. In *AISTATS*, 2019.
- Everson, R. and Roberts, S. J. Independent Component Analysis: A Flexible Nonlinearity and Decorrelating Manifold Approach. *Neural Computation*, 11(8):1957–83, 1999.
- Everson, R. and Roberts, S. J. *Independent Component Analysis*. Cambridge University Press, 2001. ISBN 9780521792981. doi:10.1017/CBO9780511624148.
- Golinski, A., Rainforth, T., and Lezcano-Casado, M. Improving Normalizing Flows via Better Orthogonal Parameterizations. In *ICML Workshop on Invertible Neural Networks and Normalizing Flows*, 2019.
- Higgins, I., Matthey, L., Pal, A., Burgess, C., Glorot, X., Botvinick, M., Mohamed, S., and Lerchner, A.  $\beta$ -VAE: Learning Basic Visual Concepts with a Constrained Variational Framework. In *ICLR*, 2017. doi:10.1177/1078087408328050.
- Hoffer, E., Banner, R., Golan, I., and Soudry, D. Norm matters: Efficient and accurate normalization schemes in deep networks. In *NeurIPS*, 2018.
- Honkela, A. and Valpola, H. Unsupervised variational Bayesian learning of nonlinear models. *NeurIPS*, 2005.
- Hyvärinen, A. and Pajunen, P. Nonlinear independent component analysis: Existence and uniqueness results. *Neural Networks*, 12(3):429–439, 1999. ISSN 08936080. doi:10.1016/S0893-6080(98)00140-3.

- Hyvärinen, A., Karhunen, J., and Oja, E. *Independent Component Analysis*. John Wiley, 2001.
- Hyvarinen, A., Sasaki, H., and Turner, R. E. Nonlinear ICA Using Auxiliary Variables and Generalized Contrastive Learning. In *AISTATS*, 2019.
- Ioffe, S. and Szegedy, C. Batch Normalization: Accelerating Deep Network Training by Reducing Internal Covariate Shift. In *Proceedings of the 32nd International Conference on Machine Learning (ICML)*, 2015. ISBN 9780874216561. doi:10.1007/s13398-014-0173-7.2.
- Johnson, W. B. and Lindenstrauss, J. Extensions of Lipschitz mappings into a Hilbert space. *Contemporary mathematics*, 26(1):189–206, 1984. doi:10.1090/conm/026/737400.
- Jutten, C. and Herault, J. Blind separation of sources, Part I: An adaptive algorithm based on neuromimetic architecture. *Signal Processing*, 24(1):1–10, 1991. ISSN 01651684. doi:10.1016/0165-1684(91)90079-X.
- Karhunen, J. Nonlinear Independent Component Analysis. In Everson, R. and Roberts, S. J. (eds.), *ICA: Principles and Practice*, pp. 113–134. Cambridge University Press, 2001.
- Khemakhem, I., Kingma, D. P., Monti, R. P., and Hyvärinen, A. Variational Autoencoders and Nonlinear ICA: A Unifying Framework. In *AISTATS*, 2020.
- Kim, H. and Mnih, A. Disentangling by Factorising. In *NeurIPS*, 2018.
- Kingma, D. P. and Dhariwal, P. Glow: Generative flow with invertible 1x1 convolutions. *NeurIPS*, 2018.
- Kingma, D. P. and Lei Ba, J. Adam: A Method for Stochastic Optimisation. In *ICLR*, 2015. URL <https://arxiv.org/pdf/1412.6980.pdf>.
- Kingma, D. P. and Welling, M. Auto-encoding Variational Bayes. In *ICLR*, 2014.
- Kingma, D. P., Salimans, T., Jozefowicz, R., Chen, X., Sutskever, I., and Welling, M. Improved Variational Inference with Inverse Autoregressive Flow. In *NeurIPS*, 2016.
- Lappalainen, H. and Honkela, A. Bayesian Non-Linear Independent Component Analysis by Multi-Layer Perceptrons. In Girolami, M. (ed.), *Advances in Independent Component Analysis*, pp. 93–121. Springer, 2000. doi:10.1007/978-1-4471-0443-8\_6.
- Lawrence, N. D. and Bishop, C. M. Variational Bayesian Independent Component Analysis. Technical report, University of Cambridge, 2000.
- Lee, T. W. and Koehler, B. U. Blind source separation of nonlinear mixing models. *Neural Networks for Signal Processing - Proceedings of the IEEE Workshop*, pp. 406–415, 1997. doi:10.1109/nnsnp.1997.622422.
- Lee, T.-W., Girolami, N., Bell, A. J., and Sejnowski, T. J. A Unifying Information-Theoretic Framework for Independent Component Analysis. *Computers & Mathematics with Applications*, 39(11):1–21, 2000.
- Li, J., Li, F., and Todorovic, S. Efficient Riemannian Optimization on the Stiefel Manifold via the Cayley Transform. In *ICLR*, 2020.
- Linsker, R. An application of the principle of maximum information preservation to linear systems. *NeurIPS*, 1989.
- Mackay, D. J. C. Maximum Likelihood and Covariant Algorithms for Independent Component Analysis. Technical report, University of Cambridge, 1996.
- Papamakarios, G., Nalisnick, E., Rezende, D. J., Mohamed, S., and Lakshminarayanan, B. Normalizing Flows for Probabilistic Modeling and Inference. Technical report, DeepMind, London, UK, 2019.
- Parra, L. Symplectic nonlinear component analysis. In *NeurIPS*, pp. 437–443, 1996.
- Parra, L., Deco, G., and Miesbach, S. Redundancy reduction with information-preserving nonlinear maps. *Network: Computation in Neural Systems*, 6(1):61–72, 1995. ISSN 0954898X. doi:10.1088/0954-898X\_6\_1\_004.
- Parra, L., Deco, G., and Miesbach, S. Statistical Independence and Novelty Detection with Information Preserving Nonlinear Maps. *Neural Computation*, 8(2):260–269, 1996. ISSN 08997667. doi:10.1162/neco.1996.8.2.260.
- Pearlmutter, B. A. and Parra, L. C. Maximum likelihood blind source separation: A context-sensitive generalization of ICA. In *NeurIPS*, 1997.
- Rezende, D. J. and Mohamed, S. Variational Inference with Normalizing Flows. In *ICML*, 2015.
- Rezende, D. J., Mohamed, S., and Wierstra, D. Stochastic Backpropagation and Approximate Inference in Deep Generative Models. In *ICML*, 2014.
- Roberts, S. and Choudrey, R. Bayesian independent component analysis with prior constraints: An application in biosignal analysis. In *Deterministic and Statistical Methods in Machine Learning, First International Workshop*, Sheffield, UK, 2004. ISBN 3540290737. doi:10.1007/11559887\_10.

- Roberts, S. J. Independent Component Analysis: Source Assessment & Separation, a Bayesian Approach. *IEEE Proceedings-Vision, Image and Signal Processing*, 145(3):149–154, 1998.
- Roweis, S. and Ghahramani, Z. A unifying review of linear gaussian models. *Neural Computation*, 11(2):305–345, 1999. ISSN 08997667. doi:10.1162/089976699300016674.
- Stiefel, E. Richtungsfelder und Fernparallelismus in n-dimensionalen Mannigfaltigkeiten. *Commentarii mathematici Helvetici*, 8:305–353, 1935.
- Taleb, A. A generic framework for blind source separation in structured nonlinear models. *IEEE Transactions on Signal Processing*, 50(8):1819–1830, 2002. ISSN 1053587X. doi:10.1109/TSP.2002.800399.
- Valpola, H., Oja, E., Ilin, A., Honkela, A., and Karhunen, J. Nonlinear blind source separation by variational Bayesian learning. *IEICE Transactions on Fundamentals of Electronics, Communications and Computer Sciences*, E86-A(3):532–541, 2003. ISSN 09168508.
- Van Den Berg, R., Hasenclever, L., Tomczak, J. M., and Welling, M. Sylvester normalizing flows for variational inference. In *UAI*, volume 1, pp. 393–402, 2018. ISBN 9781510871601.
- Winther, O. and Petersen, K. B. Bayesian independent component analysis: Variational methods and non-negative decompositions. *Digital Signal Processing*, 17(5):858–872, 2007. ISSN 10512004. doi:10.1016/j.dsp.2007.01.003.
- Woodruff, D. P. Sketching as a Tool for Numerical Linear Algebra. *Foundations and Trends in Theoretical Computer Science*, 10(2):1–157, 2014. doi:10.1561/04000000060.
- Yang, H. H., Amari, S. I., and Cichocki, A. Information-theoretic approach to blind separation of sources in nonlinear mixture. *Signal Processing*, 64(3):291–300, 1998. ISSN 01651684. doi:10.1016/S0165-1684(97)00196-5.

---

## Appendix for Learning Bijective Feature Maps for Linear ICA

---

### A. Proof of closeness to Steifel Manifold

**Theorem 2** For  $\mathbf{A}^+ = \mathbf{R}\mathbf{Q}$ ,  $\mathbf{R} \in SO(d_s)$ ,  $\mathbf{Q} \in \mathbb{R}^{d_s \times D}$ , as the Frobenius norm  $\|\mathbf{Q}\mathbf{Q}^T - \mathbf{I}\| \rightarrow 0$ , we also have  $\|\tilde{\mathbf{A}}^+ - \mathbf{A}^+\| \rightarrow 0$ , where  $\tilde{\mathbf{A}}^+$  is the projection of  $\mathbf{A}^+$  onto  $\mathcal{V}(d_s, D)$ .

**Proof** The Stiefel manifold is given by (assuming  $d_s < D$ ):

$$\mathcal{V}(d_s, D) = \{\mathbf{G} \in \mathbb{R}^{d_s \times D} : \mathbf{G}\mathbf{G}^T = \mathbf{I}\} \quad (21)$$

As (Absil & Malick, 2012) show, the unique projection  $\tilde{\mathbf{G}}$  onto this manifold of a matrix  $\mathbf{G} \in \mathbb{R}^{d_s \times D}$ , with polar decomposition  $\mathbf{U}\mathbf{P}$ , is simply  $\mathbf{U}$ .  $\mathbf{P}$  denotes a  $D \times D$  positive-semidefinite Hermitian matrix and  $\mathbf{U}$  is a  $d_s \times D$  orthogonal matrix, i.e  $\mathbf{U} \in \mathcal{V}(d_s, D)$  and has a conjugate transpose denoted  $\mathbf{U}^*$  such that  $\mathbf{U}\mathbf{U}^* = \mathbf{I}$ . As the Frobenius norm is invariant to unitary transformations, and because  $\tilde{\mathbf{G}}$  and  $\mathbf{U}$  are unitary matrices, the norm between  $\tilde{\mathbf{G}}$  and  $\mathbf{G}$  is

$$\begin{aligned} \|\mathbf{G} - \tilde{\mathbf{G}}\| &= \|\mathbf{G}\tilde{\mathbf{G}}^* - \mathbf{I}\| \\ &= \|\mathbf{U}\mathbf{P}\mathbf{U}^* - \mathbf{I}\| \\ &= \|\mathbf{U}(\mathbf{P} - \mathbf{I})\mathbf{U}^*\| \\ &= \|\mathbf{P} - \mathbf{I}\|. \end{aligned}$$

The final two equalities are due to the fact that  $\mathbf{U}^* = \mathbf{U}^{-1}$  and  $\mathbf{U}^*$  is unitary by definition.

For  $\mathbf{A}^+ = \mathbf{R}\mathbf{Q}$ , with  $\mathbf{R} \in SO(d_s)$  (the Lie group of special orthogonal matrices of dimensionality  $d_s \times d_s$ ) and  $\mathbf{Q} \in \mathbb{R}^{d_s \times D}$  because  $\mathbf{R}$  is unitary by definition, the polar decomposition of  $\mathbf{A}^+$  is simply  $\mathbf{R}\mathbf{U}\mathbf{P}$ , where  $\mathbf{U}\mathbf{P}$  is the polar decomposition of  $\mathbf{Q}$ . For a given projection  $\tilde{\mathbf{A}}^+$  of  $\mathbf{A}^+$  onto  $\mathcal{V}(d_s, D)$ , we have

$$\begin{aligned} \|\mathbf{A}^+ - \tilde{\mathbf{A}}^+\| &= \|\mathbf{R}\mathbf{U}\mathbf{P} - \mathbf{R}\mathbf{U}\| \\ &= \|\mathbf{U}\mathbf{P} - \mathbf{U}\| \\ &= \|\mathbf{U}\mathbf{P}\mathbf{U}^* - \mathbf{I}\| \\ &= \|\mathbf{P} - \mathbf{I}\|. \end{aligned}$$

Note that  $\mathbf{Q}\mathbf{Q}^T = \mathbf{U}\mathbf{P}\mathbf{P}^T\mathbf{U}^* = \mathbf{U}\mathbf{P}^2\mathbf{U}^*$  because  $\mathbf{P}$  is Hermitian. Hence:

$$\begin{aligned} \|\mathbf{Q}\mathbf{Q}^* - \mathbf{I}\| &= \|\mathbf{U}\mathbf{P}^2\mathbf{U}^* - \mathbf{I}\| \\ &= \|\mathbf{P}^2 - \mathbf{I}\|. \end{aligned}$$

$\mathbf{P}$  is positive-semidefinite and hence  $\|\mathbf{P}^2 - \mathbf{I}\| \rightarrow 0$  implies  $\|\mathbf{P} - \mathbf{I}\| \rightarrow 0$  and the distance between  $\mathbf{A}^+$  and  $\mathcal{V}(|s|, |z|)$  strictly decreases, i.e  $\|\mathbf{A}^+ - \tilde{\mathbf{A}}^+\| \rightarrow 0$ . Generally:

$$\|\mathbf{P}^2 - \mathbf{I}\| \rightarrow 0 \Leftrightarrow \|\mathbf{A}^+ - \tilde{\mathbf{A}}^+\| \rightarrow 0 \quad (22)$$

Or equivalently:

$$\|\mathbf{Q}\mathbf{Q}^* - \mathbf{I}\| \rightarrow 0 \Leftrightarrow \|\mathbf{A}^+ - \tilde{\mathbf{A}}^+\| \rightarrow 0 \quad (23)$$

Note that we can trivially show this for  $\mathbf{Q}^*\mathbf{Q} = \mathbf{P}^2$ .

Consequently better orthogonality approximations for  $\mathbf{Q}$  mean that  $\mathbf{A}^+$  lies closer to  $\mathcal{V}(|s|, |z|)$ . This manifold holds the optimal solution for decorrelating ICA matrices (Everson & Roberts, 1999).

## B. Proof of optimality

*Definition:* We say a matrix  $\mathbf{B}'$  is strictly more orthogonal than a matrix  $\mathbf{B}$  if  $\|\mathbf{B}'^T \mathbf{B}' - \mathbf{I}\| < \|\mathbf{B}^T \mathbf{B} - \mathbf{I}\|$ .

**Theorem 1** *As the Frobenius norm  $\|\mathbf{G} - \tilde{\mathbf{G}}\| \rightarrow 0$ , where  $\mathbf{G} \in \mathbb{R}^{r \times c}$  and  $\tilde{\mathbf{G}}$  is the projection of  $\mathbf{G}$  onto  $\mathcal{V}(r, c)$ ,  $\|\mathbf{G}\mathbf{X}\mathbf{X}^T \mathbf{G}^T - \mathbf{D}\| \rightarrow 0$ , where  $\mathbf{G}\mathbf{X}\mathbf{X}^T \mathbf{G}^T$  is the cross-correlation of the projection of data  $\mathbf{X}$  by  $\mathbf{G}$ , and  $\mathbf{D}$  is some diagonal matrix.*

**Proof** Let  $\mathbf{G} \in \mathbb{R}^{r \times c}$  be some projection matrix of data  $\mathbf{X}$ . We have  $\mathbf{S} = \mathbf{G}\mathbf{X}$ .

The cross-correlation is expressed as  $\mathbf{S}\mathbf{S}^T = \mathbf{G}\mathbf{X}\mathbf{X}^T \mathbf{G}^T$ . In the case where  $\mathbf{S}$  is perfectly decorrelated, we have:  $\mathbf{S}\mathbf{S}^T = \mathbf{D}^2$  where  $\mathbf{D}$  is a diagonal matrix. We know that according to [Everson & Roberts \(1999\)](#) the Stiefel manifold  $\mathcal{V}(r, c)$  (defined in Eq (21)) holds the set of all linearly decorrelating matrices. As [\(Absil & Malick, 2012\)](#) show, the unique projection  $\tilde{\mathbf{G}}$  onto this manifold of  $\mathbf{G}$  with polar decomposition  $\mathbf{U}\mathbf{P}$ , is simply  $\mathbf{U}$ . As such given any matrix  $\mathbf{G}$  we have a polar decomposition  $\mathbf{G} = \tilde{\mathbf{G}}\mathbf{P}$ , where  $\tilde{\mathbf{G}}$ , a linear decorrelating matrix, is the projection onto  $\mathcal{V}(r, c)$  and  $\mathbf{P}$  denotes a  $r \times c$  positive-semidefinite Hermitian matrix. For any matrix  $\mathbf{G}$  and its projection  $\tilde{\mathbf{G}}$  onto  $\mathcal{V}(r, c)$ , we have  $\tilde{\mathbf{G}}\mathbf{X}\mathbf{X}^T \tilde{\mathbf{G}}^* = \mathbf{D}^2$ , where  $\tilde{\mathbf{G}}^*$  is the complex conjugate of  $\tilde{\mathbf{G}}$ . Consequently, given that the Frobenius norm is unitary invariant and the fact that  $\tilde{\mathbf{G}}$  is unitary:

$$\begin{aligned} \|\mathbf{G}\mathbf{X}\mathbf{X}^T \mathbf{G}^T - \mathbf{D}^2\| &= \|\tilde{\mathbf{G}}\mathbf{P}\mathbf{X}\mathbf{X}^T \mathbf{P}^T \tilde{\mathbf{G}}^* - \mathbf{D}^2\| \\ &= \|\tilde{\mathbf{G}}\mathbf{P}\mathbf{X}\mathbf{X}^T \mathbf{P}^T \tilde{\mathbf{G}}^* - \tilde{\mathbf{G}}\mathbf{X}\mathbf{X}^T \tilde{\mathbf{G}}^*\| \\ &= \|\mathbf{P}\mathbf{X}\mathbf{X}^T \mathbf{P}^T - \mathbf{X}\mathbf{X}^T\| \\ &\leq \|\mathbf{P}^2 - \mathbf{I}\| \|\mathbf{X}\mathbf{X}^T\| \end{aligned}$$

The last line comes from the fact that  $\mathbf{P}$  is Hermitian and as such  $\mathbf{P}\mathbf{P}^T = \mathbf{P}^2$ . As  $\|\mathbf{X}\mathbf{X}^T\|$  is a constant,  $\|\mathbf{P}^2 - \mathbf{I}\| \|\mathbf{X}\mathbf{X}^T\| \rightarrow 0$  as  $\|\mathbf{P}^2 - \mathbf{I}\| \rightarrow 0$ . As shown in Eq (22)  $\|\mathbf{G} - \tilde{\mathbf{G}}\| \rightarrow 0 \Leftrightarrow \|\mathbf{P}^2 - \mathbf{I}\| \rightarrow 0$ . Consequently:

$$\|\mathbf{G} - \tilde{\mathbf{G}}\| \rightarrow 0 \Leftrightarrow \|\mathbf{G}\mathbf{X}\mathbf{X}^T \mathbf{G}^T - \mathbf{D}\| \rightarrow 0. \quad (24)$$

Note, however, that though a matrix may be decorrelating it will in general not be the optimal ICA matrix for a given dataset, though the optimal ICA matrix is itself decorrelating ([Everson & Roberts, 1999](#)).

### C. Sub- or Super-Gaussian Sources?

In classical non-linear ICA a simple non-linear function (such as a matrix mapping followed by an activation function) is used to map directly from data to the setting of the sources for that datapoint (Bell & Sejnowski, 1995). In this noiseless model, the activation function is related to the prior one is implicitly placing over the sources (Roweis & Ghahramani, 1999). The choice of non-linearity here is thus a claim on whether the sources were sub- or super- Gaussian. If the choice is wrong, ICA models struggle to unmix the data (Roweis & Ghahramani, 1999). Previous linear ICA methods enabled both mixed learning of super and sub sources (?), and learning the nature of the source (Everson & Roberts, 1999).

Here, our model abstracts away this design choice and transforms the original data such that it can be readily modelled as having either super- or sub-Gaussian sources by the linear ICA model, regardless of the true underlying sources.

### D. Identifiability of Linear ICA

Recall that for noiseless linear ICA the learnt sources will vary between different trained models only in their ordering and scaling (Choudrey, 2000; Hyvärinen et al., 2001; Everson & Roberts, 2001). Under this model our data matrix  $\mathbf{X}$  is

$$\mathbf{X} = \mathbf{A}\mathbf{S}, \quad (25)$$

where each column of  $\mathbf{S}$  is distributed according to  $p(\mathbf{s})$ . Given a permutation matrix  $\mathbf{P}$  and a diagonal matrix  $\mathbf{D}$ , both  $\in \mathbb{R}^{d_s \times d_s}$ , we define new source and mixing matrices such that  $\mathbf{X}$  is unchanged:  $\mathbf{A} \leftarrow \mathbf{A}\mathbf{P}\mathbf{D}$  and  $\mathbf{S} \leftarrow \mathbf{P}\mathbf{D}^{-1}\mathbf{S}$  (Choudrey, 2000). With fixed source variance the scaling ambiguity is removed, so linear ICA is easy to render identifiable up to a permutation and sign-flip of sources. However, this is only the case when the underlying sources are non-Gaussian (Hyvärinen et al., 2001). The Bijecta model can be interpreted as learning the “data” for linear ICA, with

$$f(\mathbf{X}) \approx \mathbf{A}\mathbf{S}. \quad (26)$$

In this setting, a natural question to ask is whether or not, given a particular function  $f : \mathcal{X} \rightarrow \mathcal{Z}$ , the linear ICA is identifiable. The Bijecta model explicitly aims to induce this linear identifiability on its feature map, as we impose a Laplace prior  $p(\mathbf{s})$ , with fatter-than-Gaussian tails.

### E. Coupling Layers in Flows

Coupling layers in flows are designed to produce lower triangular Jacobians for ease of calculation of determinants. Durkan et al. (2019) achieve this in the following fashion:

1. Given an input  $\mathbf{x}$ , split  $\mathbf{x}$  into two parts  $\mathbf{x}_{1:d-1}$  and  $\mathbf{x}_{d:D}$ ;
2. Using a neural network, compute parameters for a bijective function  $f$  using one half of  $\mathbf{x}$ :  $\theta_{d:D} = \text{NN}(\mathbf{x}_{1:d-1})$ ; parameters  $\theta_{1:d-1}$  are learnable parameters that do *not* depend on the input;
3. The output  $\mathbf{y}$  of the layer is then  $y_i = f_{\theta_i}(x_i)$  for  $i = 1, \dots, D$ .

These coupling transforms thus act elementwise on their inputs.

## F. Reconstructions and Latent Traversals

### F.1. Reconstructions



Figure F.6. Original data and reconstructions for Fashion MNIST (a)-(d), CIFAR-10 (e)-(h) and CelebA (i)-(l). The first column – (a), (e), (i) – shows a random selection of 40 images from the training set for each dataset. The second column – (b), (f), (j) – shows the reconstructions obtained by linear non-square ICA using our approximately-Stiefel unmixing matrix as in Section 5, with  $d_s = 64$  for all datasets. Note that in Fashion-MNIST the model struggles to give uniform regions of the same intensity, instead we have these bands of noise. For CIFAR-10 and CelebA much of the finer detail is lost. The third column – (c), (g), (k) – shows the reconstructions for Bijecta with an RQS flow with a single layer and  $d_s = 64$ . The fourth column – (d), (h), (l) – for a Bijecta with a four-layer RQS flow,  $d_s = 64$ . Both of these models show much higher fidelity reconstructions than the linear ICA model. They give similar quality reconstructions for Fashion-MNIST and CIFAR-10. For CelebA the difference between 1-layer and 4-layer Bijectas is more clear, with the 4-layer model giving better preservation of the identity of the person in the input image in the reconstructions.

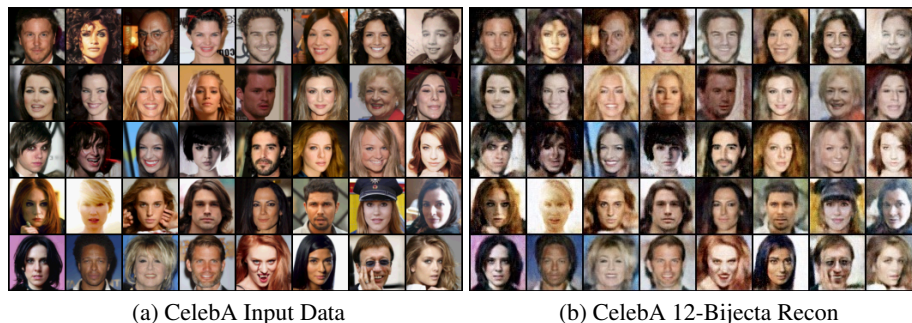


Figure F.7. Here we show reconstructions for a 12 layer Bijecta model, trained on a batch size of 64 for the CelebA dataset, with a latent space dimensionality  $d_s = 512$ . The quality of the reconstructions clearly illustrate that as we stack invertible layers our model and increase the size of  $\mathcal{S}$  we is able to reconstruct images with a high degree of accuracy.

## F.2. Latent Traversals

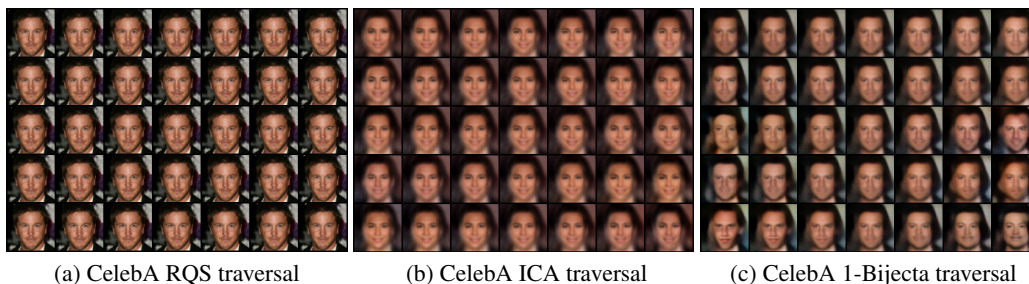


Figure F.8. Here we show latent traversals moving along the first five learnt latent directions in (a) a 4 layer RQS flow, (b) a linear ICA model with 64 latent dimensions in  $\mathcal{S}$ , and (c) a 1 layer bijecta model also with 64 latent dimensions for an embedded training-set point of the CelebA dataset. Images in the center correspond to the original embedded point. As we move to the right or left these images correspond to linearly increasing values along a single latent dimension up to 10 standard deviations away whilst the other dimensions remain fixed. It is very apparent that Bijecta is best able to learn axis-aligned transformations of the data.

## G. Network Architectures and Hyperparameters

Within all Rational Quadratic Spline (RQS) flows we parameterise 2 knots for each spline transform. The hyper-parameters of the knots were as in the reference implementation from Durkan et al. (2019), available at [github.com/bayesiains/nmf](https://github.com/bayesiains/nmf): we set the minimum parameterised gradient of each knot to be 0.001, the minimum bin width between each encoded knot and the origin to be 0.001, and the minimum height between each knot and the origin to be 0.001.

Unlike in Durkan et al. (2019), where they view a single RQS ‘layer’ as composed of a sequence of numerous coupling layers, in this paper the number of layers we describe a model as having is exactly the number of coupling layers present. So for our 4-layer models there are four rational quadratic splines. Each layer in our flows are composed of: an actnorm layer, an invertible 1x1 convolution, an RQS coupling transform and a final invertible 1x1 convolution.

The parameters of the knots were themselves parameterised using ResNets nets, as used in RealNVP (Dinh et al., 2017), for each of which we used 3 residual blocks and batch normalisation. As in Dinh et al. (2017) we factor-out after each layer. All training was done using ADAM (Kingma & Lei Ba, 2015), with default  $\beta_1, \beta_2$ , a learning rate of 0.0005 and a batch size of 512. We perform cosine decay on the learning rate during training, training for 25,000 steps.

Data was rescaled to 5-bit integers and we used RealNVP affine pre-processing so our input data was in the range  $[\epsilon, 1 - \epsilon]$  with  $\epsilon = 0.05$ .